Tropical intraseasonal oscillations as key driver and source of predictability for the 2022 Pakistan record-breaking rainfall event

npj | climate and atmospheric science

Article

Published in partnership with CECCR at King Abdulaziz University

https://doi.org/10.1038/s41612-024-00809-9

Tropical intraseasonal oscillations as key driver and source of predictability for the 2022 Pakistan record-breaking rainfall event

Jinhui Xie[1], Pang-Chi Hsu[1] ✉, June-Yi Lee[2,3], Lu Wang[1] & Andrew G. Turner[4,5]

In August 2022, Pakistan experienced unprecedented monsoon rains, leading to devastating floods and landslides affecting millions. While previous research has mainly focused on the contributions of seasonal and synoptic anomalies, this study elucidates the dominant influences of tropical and extratropical intraseasonal oscillations on both the occurrence and subseasonal prediction of this extreme rainfall event. Our scale-decomposed moisture budget analysis revealed that intense rainfall in Pakistan was triggered and sustained by enhanced vertical moisture transport anomalies, primarily driven by interactions between intraseasonal circulation anomalies and the prevailing background moisture field when tropical and mid-latitude systems coincided over Pakistan. Evaluation of subseasonal-to-seasonal prediction models further highlighted the critical role of tropical intraseasonal modes in causing this extreme rainfall event in Pakistan. Models that accurately predicted northward-propagating intraseasonal convection with a forecast lead time of 8–22 days demonstrated good skill in predicting the extreme event over Pakistan.

In August 2022, Pakistan experienced its heaviest and most persistent rainfall event of the past 60 years, with some areas receiving eight times their usual August rainfall, leading to catastrophic flooding and landslides. This affected an estimated 33 million people and severely impacted the nation's economy and infrastructure (https://floodlist.com/asia/pakistan-floods-update-august-2022). Understanding the causes behind this extreme event[1,2] and evaluating the accuracy of state-of-the-art model predictions[3–5] hold both scientific and operational importance.

The summer monsoon rainfall, occurring from July to September, serves as the primary source of annual precipitation in Pakistan. Its abnormal behavior, induced by anomalous monsoon circulation and moisture transport, often leads to floods and droughts and is regarded as a potential contributor to extreme rainfall events in Pakistan[2,6–9]. The role of sea surface temperature (SST) anomalies over the tropical Pacific and Indian Ocean in the occurrence of heavy rainfall in Pakistan has been widely discussed[5,8,10–13], particularly the La Niña and negative Indian Ocean Dipole states. Easterly wind anomalies over northern India induced by Pacific and Indian Ocean SST anomalies[1,14,15] and the southerly wind anomalies towards Pakistan from the Arabian Sea[1,16] together lead to intensified moisture convergence and strong downpours over Pakistan[17]. The high temperature and geopotential anomalies related to heatwave events in Eurasia and East Asia were found to be connected with the occurrence of Pakistan flooding in summer 2022 via teleconnections[1,14,18], and Eurasian heatwave and blocking events were also evident factors in a previous flooding event in Pakistan in 2010[19,20]. Besides seasonal anomalies, recent studies also focus on the influence of synoptic low-pressure systems, western disturbances and their interaction in South Asia[9,21,22], suggesting that their increasing intensity and duration could heighten flood risks under global warming.

Between the time scales of synoptic disturbances (<10 days) and seasonal/monsoonal anomalies (>90 days; low-frequency background state, LFBS), the intraseasonal oscillation (ISO), with a period of 10–90 days, is active over the Asian monsoon region[23–26] and tightly connected to extreme rainfall events[27,28]. Comparatively, however, the involvement of the ISO in the 2022 Pakistan rainfall event has been relatively less well explored[14]. Chen

[1]Key Laboratory of Meteorological Disaster of Ministry of Education/Joint International Research Laboratory of Climate and Environment Change/Collaborative Innovation Center on Forecast and Evaluation of Meteorological Disasters, Nanjing University of Information Science and Technology, Nanjing, Jiangsu, China. [2]Center for Climate Physics, Institute for Basic Science, Busan, South Korea. [3]Research Center for Climate Sciences and Department of Climate System, Pusan National University, Busan, South Korea. [4]National Centre for Atmospheric Science, University of Reading, Reading, UK. [5]Department of Meteorology, University of Reading, Reading, UK. ✉e-mail: pangchi@nuist.edu.cn

et al.[29] recently identified that the combination of northward-propagating ISO and the Silk Road Pattern[30,31] significantly influences extreme precipitation events in Pakistan, as observed in the summers of 2022 and 2010[18,19]. It is important to note, however, that tropical intraseasonal variability over the Asian monsoon regions encompasses two distinct modes: lower-frequency (30–60-day) and higher-frequency (10–30-day) oscillations[26,32]; and most prior research, including Chen et al.[29] focuses on the impact of the 30–60-day ISO on extreme rainfall events in Pakistan, with the potential contributions of the 10–30-day mode having been largely overlooked. Furthermore, mid-latitude wave-train patterns with intraseasonal variability have also been acknowledged as critical drivers of extreme events across Eurasia[33,34]. Similar to tropical ISOs, extratropical intraseasonal modes are complex and exhibit both quasi-biweekly and lower-frequency timescales. To date, a comprehensive understanding of the relative effects of various ISO modes, including both tropical and extratropical components, on the extreme rainfall associated with the 2022 Pakistan flooding and their key processes remains elusive.

Accurate prediction of extreme events is crucial for effective disaster mitigation. By assessing seasonal prediction systems and conducting model experiments, Dunstone et al.[3] and Doi et al.[5] unveiled the sources of predictability at the seasonal scale for the 2022 Pakistan flood event. Both studies highlighted the importance of regional SST anomalies in predicting this extreme rainfall event, though Dunstone et al.[3] highlighted the influence of La Niña, while Doi et al.[5] emphasized the impact of warming over the Arabian Sea. Malik et al.[4] found that weather prediction models can provide early warnings for rainfall over Pakistan about a week in advance. However, when it comes to predictions at the subseasonal-to-seasonal (S2S) time scales, which bridge the gap between climate prediction and weather forecasting[35], the predictability of this extreme event remains unclear. Singh et al.[36] recently developed calibrated probabilistic forecasting methods to enhance subseasonal prediction skill for events in Pakistan. However, the underlying causes of biases in the S2S prediction models during extreme events have not been analyzed, necessitating comprehensive assessments to address this issue.

To enhance our understanding of the August 2022 extreme event in Pakistan, the present study examines the impact of tropical–extratropical interactions among various intraseasonal modes. Additionally, we aimed to identify which modes are crucial for accurately predicting such an event at the subseasonal timescale. Such insights could be instrumental in identifying windows of opportunity for enhancing the subseasonal prediction of extreme events[37].

Results

Atmospheric conditions contributing to the extreme precipitation in Pakistan

The temporal evolutions of rainfall in Pakistan recorded by rain-gauge-based data (CPC; Fig. 1a) and high-resolution (0.25°) ERA5 data (Fig. 1b) are displayed and compared. Both datasets revealed the extremely large amplitude of rainfall amounts (red bars) relative to the climatological state (pink bars) during the period of flood occurrence (August 12–26, 2022). The daily rainfall anomalies (red minus pink bars; black curves in lower panels) averaged over the flooding period were 12.5 mm d^{-1} and 9.5 mm d^{-1}, which are about 6.8 and 3.7 standard deviations larger than the corresponding climatological means derived from the CPC and ERA5, respectively.

Notably, enhanced rainfall persisted throughout the flood period, although its amplitude showed fluctuations, with two extremes on 17 and 24 August. The fluctuating characteristics reflected the multiscale variations of Pakistan rainfall (curves with different colors in the lower panels of Fig. 1a, b). By employing the temporal decomposition approach for rainfall time series at each grid cell, we can compare the contributions of variability at various time scales to the spatial pattern of total rainfall anomalies (Figs. S1, S2 in the supplemental material) and quantify their area-average effect within Pakistan (Fig. 1a, b). The yellow curve fluctuations in the lower panels of Fig. 1a, b depict the high-frequency (< 10 days) variability. They align closely with the two peak periods of summer rainfall in Pakistan (17 and 24 August), capturing the movement of tropical depression systems (BOB 06 and 07) as they travel from the Bay of Bengal towards Pakistan (Figs. S1–S2). However, the contribution of synoptic rainfall anomalies to the total rainfall during the entire flood period from 12 to 26 August is relatively minor, accounting for approximately 4% (as indicated by the yellow characters on the left in both panels). This is because positive effects being present only on limited days (Fig. S1) and over limited areas (Fig. S2a1–a6). Most days without tropical depressions, which correspond to drier conditions, were considered to have made a negative contribution to the rainfall anomalies associated with this heavy rainfall event.

Unlike the synoptic effects, the LFBS component of Pakistan rainfall consistently remained positive throughout the summer of 2022 (brown curves in Fig. 1a, b). This component accounted for nearly 40% of the total rainfall during the flooding period, as denoted by the brown characters. Since the LFBS encompasses all components with periods longer than 90 days, including long-term trends related to anthropogenic activity and internal interannual-decadal variability, we analyzed the connection between the LFBS and Pakistan rainfall using both un-detrended and detrended data for the summer season (Fig. S3). As found by previous studies[18], Pakistan rainfall during the monsoon season is negatively correlated with ENSO (Fig. S3a) through inducing an easterly wind anomaly that transports moisture into the Indian monsoon area (Fig. S3b). Recent studies have also highlighted the significant impact of the La Niña state on several extreme events in Asia, including the 2022 summer flooding in Pakistan and heatwave in the Yangtze River basin[1,17].

Beyond the contributions of synoptic-scale (<10 days) and LFBS (>90 days) components, approximately 56–60% of the rainfall associated with the Pakistan flood originated from the two ISO modes. Both the 10–30-day (green curves) and 30–90-day (blue curves) rainfall variations display a positive phase during the heavy rainfall period (August 12–26, 2022), in contrast to the negative phases observed before and after the flooding (lower panels of Fig. 1a, b). This pattern suggests that ISO variations are closely linked with the alternating dry and wet phases of rainfall variability in Pakistan during the summer of 2022, as indicated by Chen et al.[29]. The active ISO activities also created favorable conditions for increased synoptic variability. In essence, ISOs play a critical role in triggering and modulating the occurrence of heavy rainfall.

The simultaneous effects of components from different timescales (Fig. 1a, b) also imply the potential existence of multi-scale interactions. The nature of these interactions and their collective impact on the heavy rainfall event were examined through the moisture budget equation and the associated scale-decomposed method, as detailed in Eqs. (1) and (2). The moisture tendency (black curve in Fig. 1c) showed a positive value before the peaks of rainfall on 17 and 24 August (blue curve in Fig. 1c) but turned to a negative value afterward, suggesting the accumulation of moisture was crucial for the occurrence of downpours. The dominant contributor to the moisture source was vertical moisture advection (red curve), although it tended to be offset partly by condensation processes (yellow curve). The effect of horizontal moisture advection was relatively small (green curve) compared to the other budget terms. Thus, the variations in rainfall (blue curve) most closely followed those in vertical moisture advection ($-\omega\frac{\partial q}{\partial p}$).

To further understand the relative contributions from different scale-interaction processes, we computed the individual terms of the scale-decomposed vertical advection process [Eq. (2)]. As shown in Fig. 1d, both reanalysis datasets revealed that the leading processes ($-\bar{\omega}\frac{\partial \bar{q}}{\partial p}$, $-\omega'\frac{\partial \bar{q}}{\partial p}$, $-\omega''\frac{\partial \bar{q}}{\partial p}$ and $-\omega^*\frac{\partial \bar{q}}{\partial p}$) were related to the vertical transportation of LFBS moisture by various timescale components. With a focus on the origin of the ascending motion anomaly during the flooding period (Fig. S4), we compared the evolutions of vertical motion under different time scales (Figs. S4a–d). Among them, the synoptic-scale ascending motion anomalies were strong on 17 and 24 August when tropical depressions approached Pakistan (Fig. S1), while they exerted a negative (descending or drying) effect during the dates without the influences of synoptic depression systems (Fig. S4a). The vertical motion anomaly associated with the > 90-day background state

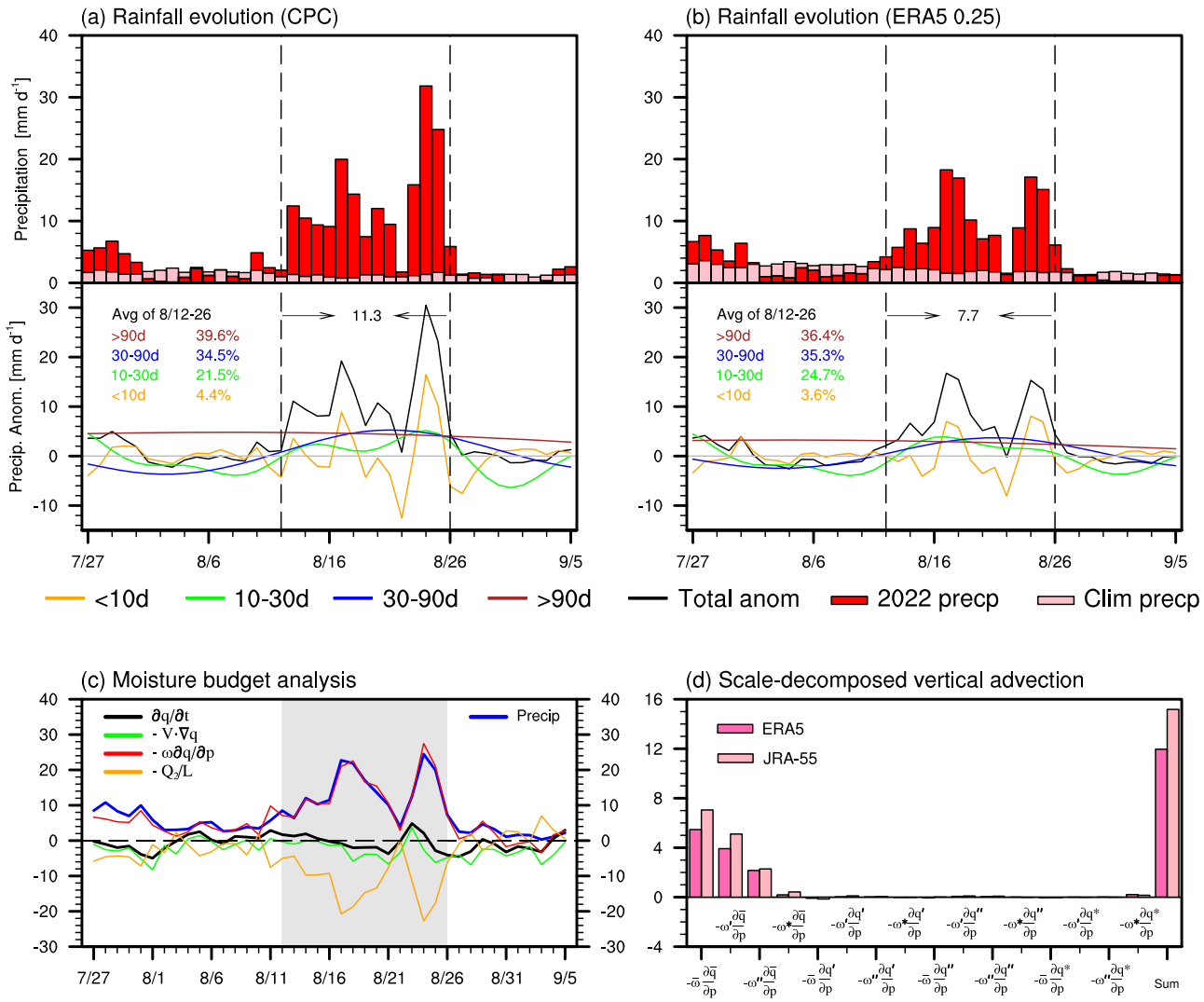

Fig. 1 | Time evolution of 2022 Pakistan rainfall and associated moisture budget analysis. a (Top) Daily rainfall amount (red bars; units: mm d^{-1}; left-hand *y*-axis) from 27 July to 10 September 2022 (*x*-axis in dates) compared with the climatological daily mean (pink bars; units: mm d^{-1}; left-hand *y*-axis) in 1980–2022 within Pakistan territory derived from the CPC. (Bottom) The different timescale components of Pakistan rainfall (units: mm d^{-1}; right-hand *y*-axis) are displayed by the curves of various colors in the upper part of this panel: synoptic component (< 10 days; yellow curves); 10–30-day (green curves); 30–90-day (blue curves); and LFBS (>90 days, brown curves). Their ratios to the total precipitation during the flooding period (i.e., the black number within the two dashed lines of 12 and 26 August) are shown by the percentages in corresponding colors. **b** as in (**a**) but for the results derived from the high-resolution (0.25°) ERA5. **c** Evolution of rainfall rate (units: 10^{-5} mm s^{-1}; right-hand *y*-axis) and column-integrated (surface to 300 hPa) the moisture budget terms (units: 10^{-5} kg m^{-2} s^{-1}; left-hand *y*-axis) over the territory of Pakistan derived from ERA5. Blue, black, green, red, and yellow lines denote the variations of rainfall rate, $\partial q/\partial t$, $-V \cdot \nabla q$, $-\omega \partial q/\partial p$, respectively. The gray shading marks the time span of the flooding event. **d** Individual terms of vertical moisture advection resulting from scale-interaction processes (16 terms on the r.h.s. of Eq. 2) and their summation (the rightmost term) derived from ERA5 (dark pink bars) and JRA-55 (light pink bars). Units: 10^{-5} kg m^{-2} s^{-1}.

maintained a positive contribution throughout August 2022 (Fig. S4d). The activities of the two ISO modes generated ascending motion anomalies during the period of heavy rainfall and underwent a phase transition around the onset and end of the event (Figs. S4b, c). The evolution of vertical motion (Fig. S4) is highly consistent with the features of rainfall variation shown in Fig. 1a, b, confirming the superposed modulating effects of different time-scale circulation anomalies on the Pakistan extreme rainfall. The two ISO modes were indeed important in regulating the occurrence of the heavy rainfall that caused the 2022 Pakistan flooding event.

The next question is where the 30–90-day and 10–30-day perturbations that favored the Pakistan extreme rainfall came from. Did they appear locally (i.e., regional oscillatory modes) or move from other regions (i.e., propagating modes)? From the OLR evolution maps, tropical–extratropical coupling of intraseasonal modes is clear over 60°–80°E (Fig. 2a, f). The northward-propagating 30–90-day convection was initiated over the equatorial Indian Ocean in early August and arrived in Pakistan (area between the two green lines) during the flooding period (the period between the two dashed black lines); meanwhile, the mid-latitude 30–90-day variability also moved southwards towards Pakistan (Fig. 2a). These 30–90-day convective anomalies were associated with enhanced ascending motion. The profiles of vertical motion also capture the coupling of tropical and extratropical 30–90-day modes (Fig. 2b–d), which resulted in the occurrence of heavy rainfall when the convective and upward motion anomalies appeared over Pakistan (Fig. 2e). In contrast, the 10–30-day convective and ascending motion anomalies favoring the rainfall occurrence over Pakistan were mainly from the tropics. They moved northwards from the equatorial area from early August and reached Pakistan during the flooding period (Fig. 2f–j). The southward-propagating quasi-biweekly ISO seemed to meet with tropical signals over the northern area of Pakistan in late August when the flood event ended (Fig. 2f). This suggests that the northward movement

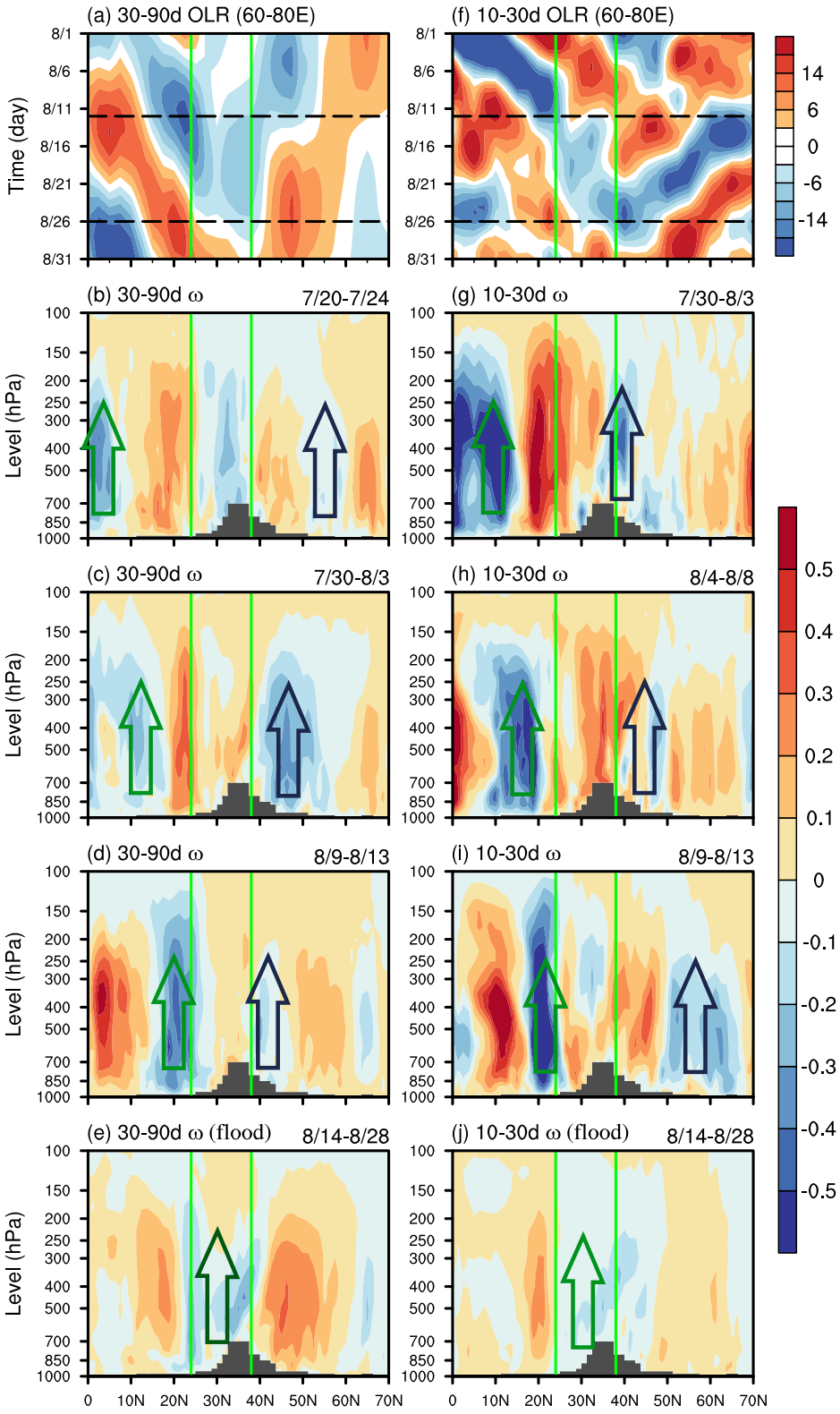

Fig. 2 | Evolution of ISO convection and circulation before and during the Pakistan extreme rainfall event. a Latitude–time diagram of 30–90-day OLR anomalies (units: W m^{-2}) averaged along 60°–80°E during August 2022. Latitude is shown on the *x*-axis, while time is displayed on the *y*-axis. **b–d** Latitude–height profiles of pentad composited 30–90-day *p*-velocity (units: 10^{-1} Pa s^{-1}) during 20–24 July (pentad 41), 30 July–3 August (pentad 43), and 9–13 August (pentad 45) in 2022, respectively. **e** as in (**b–d**) but for the result averaged during the flooding period (14–28 August; pentads 46–48). (Right) Similar to the left-hand panels but for the results of 10–30-day components: **g–j** 30 July–3 August (pentad 43); 4–8 August (pentad 44); 9–13 August (pentad 45); and 14–28 August (pentads 46–48), respectively. Vertical green lines mark the latitudinal location of Pakistan. Horizontal dashed black lines in (**a**) and (**f**) indicate the beginning and end of the extreme rainfall event. The green and blue arrows represent ascending motion anomalies from the tropics and mid-latitude regions, respectively. Dark shading shows the area's topography.

of tropical 10–30-day convections may have been more important than the mid-latitude 10–30-day mode for triggering and maintaining this extreme rainfall event.

The geographical evolution of the tropical and extratropical ISO modes provides a more comprehensive view of their impacts on the heavy rainfall associated with floods in Pakistan. The left- and right-hand panels of Fig. 3 (Fig. S5) display the spatiotemporal evolution of tropical and extratropical 30–90-day (10–30-day) ISO-related perturbations, respectively. Around five pentads (pentad 41) prior to the onset of flooding during 14–28 August (pentads 46–48) 2022, the 30–90-day convective and circulation anomalies exhibited a wave-train pattern, with enhanced convection/cyclonic flow over the central equatorial Indian Ocean and a suppressed/anticyclonic anomaly over the Arabian Sea and Bay of Bengal (Fig. 3a). This wave train propagated northwestward from pentad 43 to pentad 45 just before the

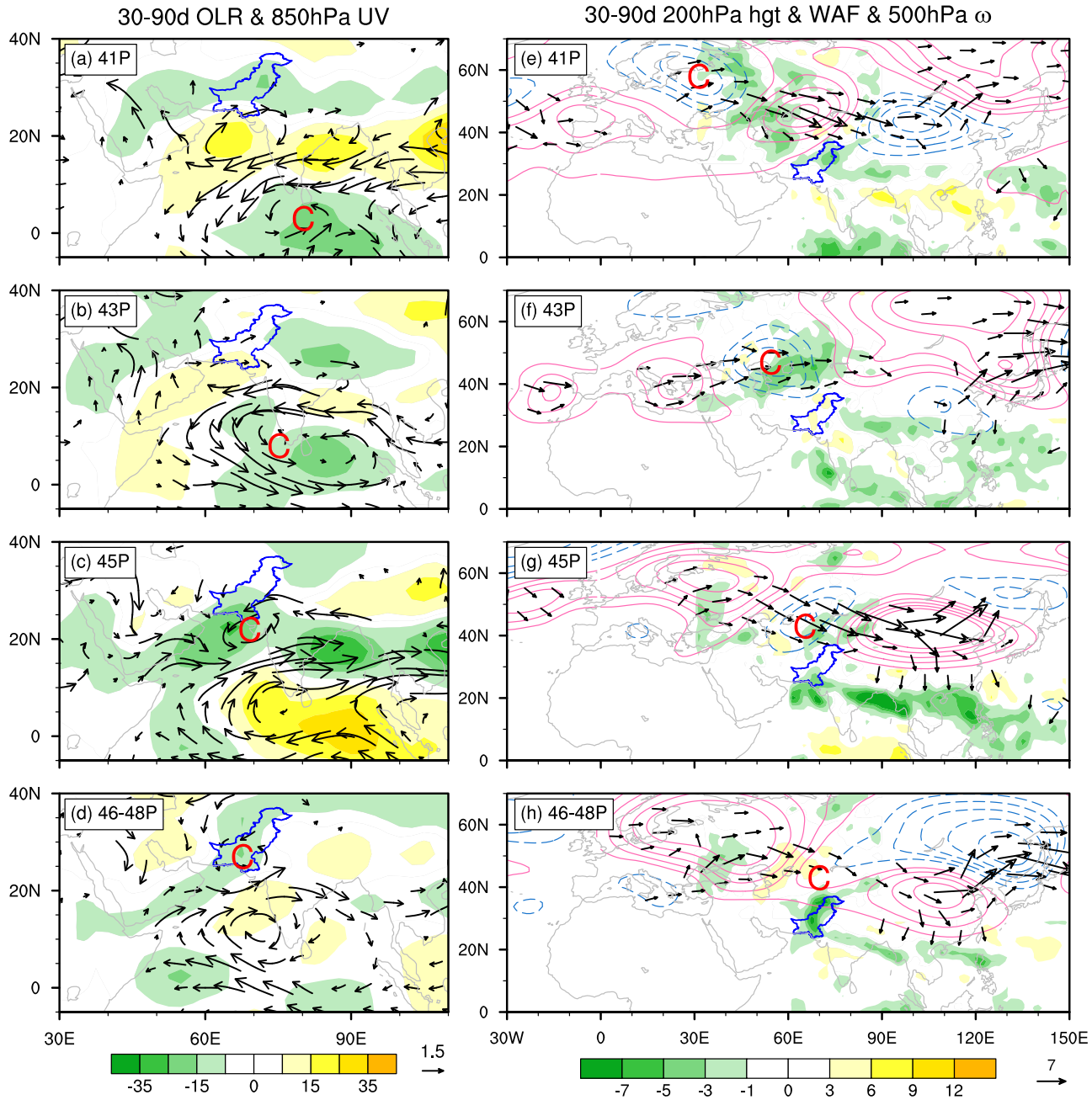

Fig. 3 | Spatiotemporal evolutions of tropical and extratropical 30–90-day variability during the 2022 Pakistan extreme rainfall event. a–d Composites of 30–90-day OLR anomalies (shading; units: W m^{-2}) and 850-hPa wind anomalies (vectors; units: m s^{-1}; only wind speeds greater than 0.5 m s^{-1} are shown) at pentads 41 (20–24 July), 43 (30 July–3 August), 45 (9–13 August), and 46–48 (14–28 August), respectively. **e–h** As in (**a–d**) but for the composites of 30–90-day geopotential height anomalies at 200 hPa (contours with an interval of 10 from −100 to 100; units: gpm), WAF at 200 hPa (vectors; units: m^2 s^{-2}; only values greater than 3 m^2 s^{-2} are shown), and *p*-velocity anomalies at 500 hPa (shading; units: 10^{-2} Pa s^{-1}). The boundary of Pakistan is outlined in blue in (**a–d**). Red letter "C" indicates the center of the cyclonic/low-pressure anomalies.

flood occurrence (Fig. 3b, c). The convective anomaly arrived and stalled in Pakistan during pentads 46–48 (Fig. 3d), accompanied by enhanced ascending motion (Fig. 2e) that led to heavy precipitation (Fig. 1). The southward movement of 30–90-day ascending anomalies from the mid-latitudes eventually merged with tropical convection over Pakistan (Fig. 2b–e) and was related to the low-frequency Rossby wave train prevalent over the mid-to-high latitude regions (Fig. 3e–h). The low-pressure anomaly (light blue dashed contour labeled "C"), a part of the Rossby wave train, seemed to originate from northern Europe (Fig. 3e) and propagated southeastward across Eurasia (Fig. 3f, g). The low-pressure anomaly associated with the mid-latitude Rossby wave train coupled with the cyclonic anomaly related to tropical ISO convection and formed persistent deep convection over Pakistan during the flooding period (Figs. 2e, 3d, h).

The evolution of tropical 10–30-day variability showed a similar feature to the 30–90-day ISO mode; both modes displayed evident northwestward propagation from the equatorial Indian Ocean toward Pakistan (Figs. S5a–d). In contrast, the extratropical 10–30-day wave-train pattern exhibited less organized evolution and weakened significantly during the flooding period (Figs. S53–h). This confirms the findings of Fig. 2 that the tropical convective and circulation anomalies played a more crucial role in triggering the Pakistan heavy precipitation than the extratropical signals associated with the 10–30-day variability.

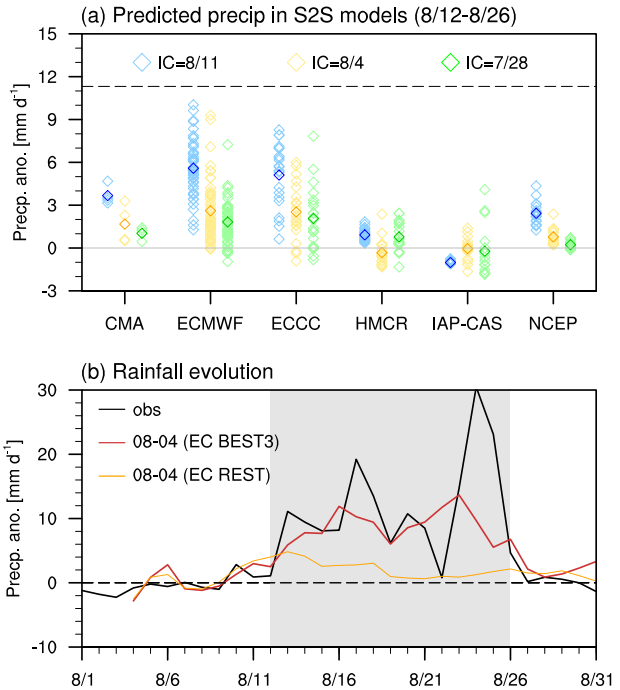

Fig. 4 | Prediction skills of Pakistan rainfall associated with 2022 flooding event by the S2S models. a Precipitation anomalies (*y*-axis; units: mm d^{-1}) for 12–26 August 2022 averaged in the territory of Pakistan predicted by six S2S models (*x*-axis). The dashed black line denotes the observed rainfall anomaly relative to the climatological daily mean. The light blue, yellow and green diamonds represent the forecasts by individual members initialized on 11 August, 4 August, and 28 July 2022, respectively. The diamonds with dark colors show the corresponding ensemble-mean results. **b** Temporal evolution of observed and predicted rainfall anomalies (*y*-axis; units: mm d^{-1}) during August 2022. The black line shows the observation, while dark red and orange lines represent the predictions of the three members with the best skill (BEST3) and the remaining 48 members (REST) from the ECMWF system initialized on 4 August 2022, respectively. Gray shading marks the time span of the occurrence of heavy precipitation in Pakistan.

So far, we have quantified and discussed the relative contributions of various ISO modes in triggering the persistent heavy rainfall over Pakistan, primarily based on a moisture budget analysis. To further understand the moistening effects driving this heavy rainfall event, we analyzed the evolution of convective instability induced by different ISO modes (Figs. S6–S8). The troposphere exhibited relatively unstable conditions, with higher instability observed in early August before the flood occurred (blue shading in Fig. S6a), during which moisture accumulated in the lower troposphere, coupled with dry conditions at mid-high levels (Fig. S6b). As persistent rainfall began, ascending convective motion continued to transport moisture upward, warming the mid-upper troposphere due to latent heat release (Fig. S6b). The troposphere became more stable, as indicated by a declining instability index during the flooding period (gray shading in Fig. S6a). While the background monsoon flow likely maintained instability throughout the summer (red curve in Fig. S6a, Fig. S6f), temporal fluctuations in instability were modulated by perturbations on different timescales (yellow, green, and blue curves in Fig. S6a). Among these, both the 10–30-day and 30–90-day components positively contributed to increased instability during the pre-flooding period, as their θ_{se} anomalies decreased with height (Figs. S6d, S6e). Notably, the 30–90-day component had a larger and more persistent effect than the 10–30-day component.

The formation of 30–90-day θ_{se} profiles was linked to the coupling effects of tropical and extratropical ISO activities. During the pre-conditioning stage, the tropical 30–90-day ISO facilitated northward moisture transport and accumulation in the lower troposphere over Pakistan, leading to low-level moistening and warming (Figs. S7a–S7b, S8a–S8e). Meanwhile, the intrusion of 30–90-day dry and cold anomalies at mid-high levels further enhanced atmospheric instability (Figs. S7a, S7b). For the 10–30-day modes, the moistening effect was also driven by the tropical mode (Figs. S8f–j), but it resulted in a shorter duration of moisture accumulation and a smaller contribution to instability during the pre-conditioning stage (Figs. S6a, S6d).

In summary, the results underscore the significance of prevailing background conditions associated with the La Niña state and their interaction with ISO variability in causing the prolonged heavy precipitation in Pakistan during the summer of 2022, with the two peaks in rainfall amounts also receiving contributions from tropical depressions. Specifically, the seasonal anomalies linked to ENSO created a favorable environment with increased moisture over the Indian Ocean. Once the ISO-related convection and cyclonic anomalies propagated from the tropics towards Pakistan, they facilitated low-level moistening. The mid-latitude ISO, with less moisture, contributed to cold air intrusion at the mid-higher troposphere. Together, these processes enhanced tropospheric instability, triggering heavy rainfall events. During the flooding period, ISO convective and ascending anomalies dominated the Pakistan region, resulting in enhanced vertical advection of moisture, which continuously fueled the rainfall. As these ISOs weakened or shifted away from the Pakistan area, the heavy rainfall began to cease.

Prediction Skills and Sources of Biases Revealed by the S2S Models

Accurately predicting persistent heavy rainfall is key to mitigating the hazards of flooding, but it poses a challenge when attempting forecasts at a long lead time beyond 10 days[4,38]. By using state-of-the-art operational models that provide real-time forecasts at the S2S timescale, we explored possibilities for predicting the amounts of persistent heavy rainfall over the flooding period from 12 to 26 August 2022 (Fig. 4a). The different color diamond markers represent the rainfall amounts in Pakistan predicted by individual members of operational prediction systems at various forecast lead times. In comparison to the observed rainfall amount (dashed black line in Fig. 4a), all members from these operational models tended to consistently underestimate the persistent heavy rainfall (diamond markers in Fig. 4a). In general, the predicted rainfall amounts at a shorter forecast lead time, such as those initialized on 11 August (strictly, forecast 2–16 days in advance relative to the target periods of 12–26 August; simply referred to as the one-week-lead forecast; light blue markers), show a smaller bias in terms of rainfall amounts compared to those with longer forecast lead times (initialized on 4 August and 28 July, represented by yellow and green markers, respectively) at around 2–3 weeks ahead. For example, the ensemble-mean prediction results initialized on 11 August by the CMA, ECMWF, ECCC, HMCR, and NCEP models indicate enhanced rainfall amounts in Pakistan (dark blue markers). However, only some members of ECMWF and ECCC capture larger positive rainfall anomalies in Pakistan in forecasts with the initialization date of 4 August (light yellow markers). The amplitude of persistent rainfall anomalies reduces when ECMWF and ECCC are initialized on 28 July (light green markers), while other models (CMA, HMCR, IAP-CAS and NCEP) fail to predict increased rainfall in Pakistan at such a lead time.

To further understand predictability beyond 10 days and identify sources of biases, we conducted a detailed analysis of prediction data from the ECMWF system, focusing particularly on ensemble members initialized on 4 August. As displayed in Fig. 4a, certain members of the ECMWF model effectively predicted enhanced rainfall amounts during the Pakistan flooding period, despite an underestimation in the all-member ensemble results. Thus, we selected the top three members with the smallest biases relative to observed rainfall amounts—referred to as the BEST3 predictions—and compared their results with the average of the remaining 48 members, referred to as the REST predictions (Fig. 4b). As expected, the BEST3 predictions (red line in Fig. 4b) more accurately captured the persistence and intensity of Pakistan's rainfall compared to the REST predictions (orange line in Fig. 4b). However, it remains challenging to predict the precise timing of maximum rainfall occurrence.

Based on the moisture diagnosis results using observational data (Fig. 1d), the occurrence of persistent heavy precipitation was greatly influenced by the vertical advection of LFBS moisture induced by ISO-related perturbations. The analysis of whether this key process also determines the prediction skill for Pakistan's rainfall is presented in Fig. 5, where we compare the associated fields in both BEST3 and REST predictions. As the distributions of LFBS moisture fields were well predicted by ECMWF (Fig. S9), we focus mainly on the predicted features of various ISO variabilities. For the tropical 30–90-day ISO, the location and intensity of ISO signals predicted by BEST3 (Fig. 5a) closely resemble the observations (Fig. 3d), depicting convective and cyclonic anomalies over Pakistan during the heavy rainfall period. In contrast, the convective/cyclonic anomalies predicted by REST appear weak and confined to the southern sector of Pakistan (Fig. 5c), indicating a failure of REST to predict the northward-propagating 30–90-day ISO and resulting in underestimation of rainfall amounts induced by active ISO phases. Regarding the 30–90-day ISO wave train over the mid-latitude regions, we found that neither BEST3 nor REST predictions capture the ascending motion in the upper troposphere over Pakistan (Fig. 5b, d). Similar to the predicted results of 30–90-day components, the convective and cyclonic anomalies associated with the tropical 10–30-day modes predicted by BEST3 (Fig. 5e) are stronger than those in the REST prediction (Fig. 5g) when compared to observations (Fig. S4d). Mid-latitude 10–30-day Rossby wave patterns seem to be insignificant in both prediction cases (Fig. 5f, h). These results suggest that the biases in predicted persistent heavy rainfall over Pakistan primarily stem from the accuracy of models in predicting tropical ISO modes. Even when the models fail to predict the mid-latitude ISO variability, they can capture enhanced rainfall in Pakistan as long as the tropical ISO convection and circulation perturbations are well predicted.

To confirm the findings from Fig. 5, we compare the vertical cross sections of vertical motion anomalies predicted by BEST3 and REST with observations in Fig. 6. Again, the observations show a consistent coupling of tropical and extratropical ISOs at the 30–90-day timescale, coinciding with heavy rainfall in Pakistan (Fig. 6a). Meanwhile, the arrival of 10–30-day ascending motion anomalies is observed to be conducive to heavy rainfall occurrence, regardless of the extratropical mode being located to the north of Pakistan (Fig. 6d). The upward motions of both the 30–90-day and 10–30-day modes of variability exhibit a distinct northward propagating feature from the tropics towards Pakistan, as predicted by the BEST3 models (Fig. 6b, e). In contrast, these features are poorly predicted by REST (Fig. 6c, f). Even in the absence of southward-moving low-frequency Rossby wave trains, the BEST3 predictions still show larger rainfall amounts in Pakistan than those predicted by REST when the moisture can be efficiently transported by tropical ISO perturbations (Fig. S10). Note that the critical contributions of tropical 30–90-day variability to the subseasonal predictability of heavy rainfall in Pakistan, as detected by comparisons between the results from good and poor members of ECMWF, are robust regardless of the specific members or models used. The predicted rainfall biases in Pakistan show the highest correlation with the fidelity of predicted 30–90-day ISO evolution over the tropics, as demonstrated across 128 members from six S2S models (Fig. S11).

The slight underestimation of extreme rainfall amplitude in BEST3 could be attributed to the model's limitation in accurately capturing synoptic systems (Fig. S12). The results highlight that, for the 2022 Pakistan flooding event, the major sources of Pakistan rainfall predictability at the extended-range timescale are the tropical ISO signals at both 30–90-day and 10–30-day time scales.

Discussion

Based on the observational diagnosis, our findings emphasize the role of northward-propagating 30–90-day and 10–30-day ISO perturbations from the tropics towards Pakistan in inducing this persistent heavy rainfall event during mid to late August 2022. Model prediction assessments further suggest that the major source of subseasonal predictability for this event is the tropical 30–90-day ISO.

Although our results highlight the importance of accurate predictions of tropical ISO evolution for forecasting heavy rainfall in Pakistan, identifying the factors that significantly affect the fidelity of convective perturbation predictions remains a critical but complex issue. To provide insights for model improvement, we discuss the potential effects of the models' physical frameworks and settings. Since all the models considered are hydrostatic (Table S1) but have varying horizontal resolutions, we analyzed predicted rainfall amounts for Pakistan during the flooding period by higher and lower-resolution models at different initialization dates (Fig. S13a). As expected, higher-resolution models demonstrate better capability in capturing enhanced rainfall anomalies (blue boxplots) compared to lower-resolution models (yellow boxplots), which generally predict smaller anomalies. Additionally, these six S2S models employ different approaches for data assimilation and convective parameterizations (Table S1). Given the diverse and complex nature of these parameterizations, which are not easily categorized, we examined the effects of data assimilation methods (Fig. S13b). The results indicate that rainfall predictions are not significantly sensitive to the data assimilation approaches used. Therefore, a more thorough and systematic evaluation of how model parameters affect subseasonal predictions will be a key focus of our future work.

The current study on this unique event also prompts some intriguing questions regarding monsoon dynamics. For example, one may wonder why such a prolonged (lasting about two weeks) extreme rainfall event has not commonly occurred in the core monsoon region, where more moisture is available. We identified and analyzed one long, sustained (15-day) extreme event over western India and found that tropical intraseasonal perturbations indeed contribute positively by providing abundant moisture. However, mid-latitude intraseasonal signals showed minimal effect, as they seem to rarely extend to such southern latitudes. As previously discussed, the anomalous cold air intrusion may have increased instability during the pre-flooding period of the Pakistan event (Figs. S6, S7). Further research is needed to clarify the extent to which tropical–extratropical interactions contribute to the persistence of heavy rainfall over South Asia by systematically analyzing all historical extreme events.

Considering that Pakistan is located north of the core monsoon region, the following question arises: Was the simultaneous northward movement of the enhanced 30–90-day and 10–30-day convections toward Pakistan unique? Was this driven by certain physical processes, or was it simply a stochastic instance? In fact, not all the ISOs tended to propagate as far north (24°N) as Pakistan is situated and it is also uncommon for both ISO modes to be simultaneously enhanced and to reach Pakistan during the same period. In future work, we plan to investigate the dynamics of tropical ISO diversity over the South Asian summer monsoon region, as this appears to be a key mechanism influencing the frequency of extreme events in the northern Indian subcontinent. In addition, we will examine how ISO diversity impacts subseasonal prediction skills for extreme events over the South Asian monsoon area in operational models.

Materials and methods

Datasets

To reduce the uncertainty, we collected three sets of gridded precipitation data: (1) daily mean precipitation data with a horizontal resolution of 0.5° × 0.5° from the National Oceanic and Atmospheric Administration's (NOAA's) Climate Prediction Center (CPC)[39]; (2) daily-averaged precipitation data from the fifth major global reanalysis produced by ECMWF (ERA5)[40] with a horizontal resolution of 0.25° × 0.25°; and (3) three-hourly precipitation data from the Japanese 55-year reanalysis (JRA-55)[41] dataset with a horizontal resolution of 1.25° × 1.25°. The daily outgoing longwave radiation (OLR) from NOAA[42] on a 2.5° × 2.5° grid was used to analyze the variability and distribution of deep convection. The status of El Niño–Southern Oscillation (ENSO) was provided by NOAA's Physical Sciences Laboratory (https://psl.noaa.gov/gcos_wgsp/Timeseries/Data/nino34.long.data), defined by the Niño3.4 SST index calculated by the Hadley Center Sea Ice and Sea Surface Temperature dataset (HadISST1)[43]. The daily zonal and meridional (u and v) winds, vertical p-velocity (ω),

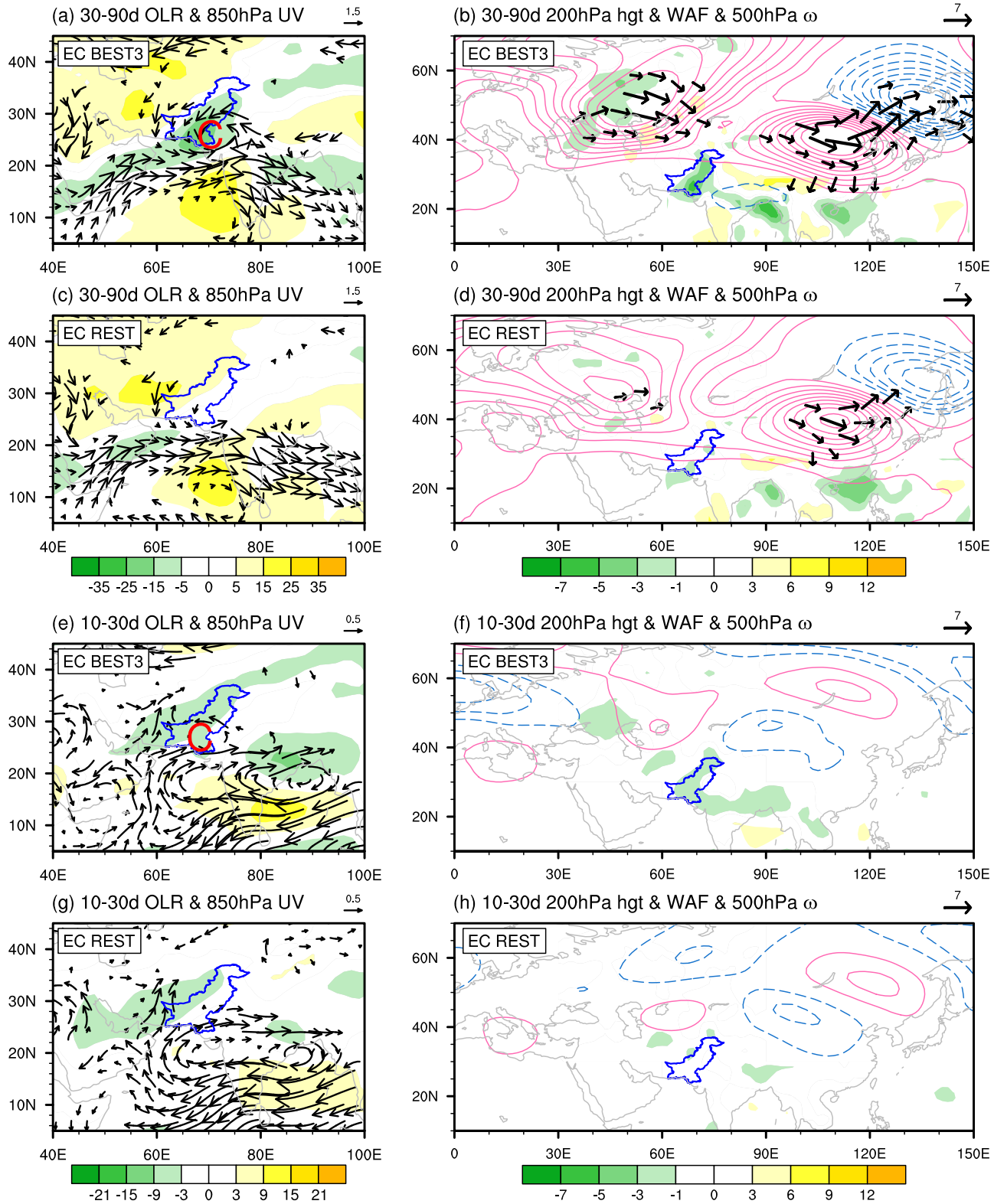

Fig. 5 | Tropical and extratropical intraseasonal signals during the 2022 Pakistan flooding event predicted by the good and poor members of ECMWF model. As in the bottom panels of Fig. 3 but for the ECMWF ensemble predictions from (**a**, **b**) BEST3 and (**c**, **d**) REST, initiated on 4 August 2022. The target period is 12–26 August 2022. **e**–**h** Similar to (**a**–**d**) but for the composite results of predicted 10–30-day perturbations.

specific humidity (q), and geopotential height (Z) from 1000 to 100 hPa were obtained from the ERA5 and JRA-55 datasets to enhance the robustness of large-scale composite results. Both datasets were available at a resolution of 1.25° × 1.25°, for understating the anomalous dynamic and thermodynamic conditions during this flooding event in Pakistan. JRA-55 covers the period 1981–2022, while the other datasets span 1980–2022.

For the prediction products from operational models, we collected real-time forecast and reforecast data from the S2S database coordinated by the World Meteorological Organization S2S prediction

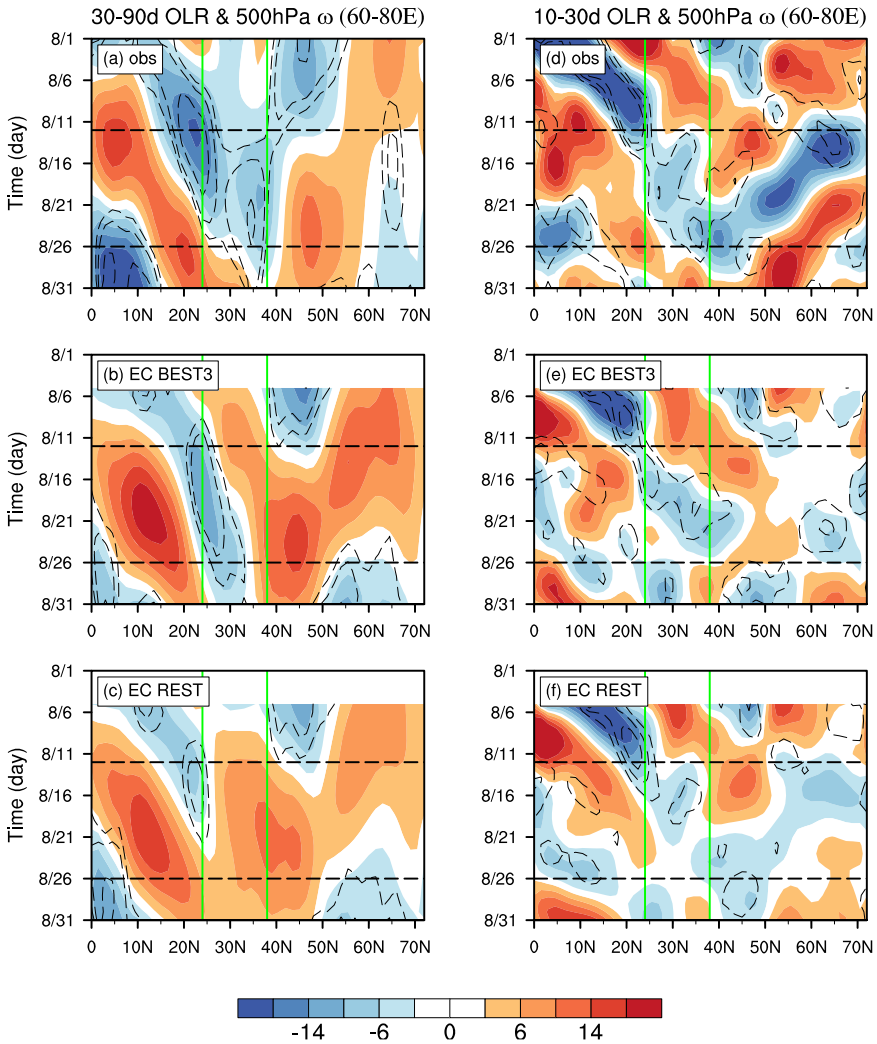

Fig. 6 | Evolution of intraseasonal signals predicted by the good and poor members of ECMWF model. a Latitude–time evolution of observed 30–90-day OLR anomalies (shading; units: W m^{-2}) and *p*-velocity anomalies at 500 hPa (contours; units: 10^{-2} Pa s^{-1}; intervals: −3.2, −1.6, −0.8) averaged between 60°E and 80°E in August 2022. **b**, **c** As in **a** but for the ECMWF predictions initialized on 4 August 2022 for BEST3 and REST, respectively. **d**–**f** Similar to (**a**, **b**) but for the composite results of predicted 10–30-day perturbations, in which the contours in (**d**–**f**) represent vertical velocities of −0.05, −0.03 and −0.01 Pa s^{-1}. The vertical green solid lines mark the region of Pakistan. The horizontal black dashed lines indicate the beginning and end of the extreme precipitation event in Pakistan.

project[33]. We selected data from six operational models, ensuring they were initialized on similar dates to facilitate systematic comparisons. These models were those of the China Meteorological Administration (CMA), Environment and Climate Change Canada (ECCC), the ECMWF, the Hydrometeorological Center of Russia (HMCR), the Institute of Atmospheric Physics–Chinese Academy of Sciences (IAP-CAS), and the National Centers for Environmental Prediction (NCEP). Table 1 provides further details of these models and their related forecast information.

Diagnosis of moisture budget equation

To understand the physical processes responsible for the heavy rainfall event, the moisture budget equation[44] and its scale-decomposed terms were analyzed. As shown in Eq. (1), the changes in specific humidity (q) at a constant pressure level are determined by three processes: horizontal moisture advection, vertical moisture advection, and the moisture sink (Q_2),

$$\frac{\partial q}{\partial t} = -\boldsymbol{V}\bullet\nabla q - \omega\frac{\partial q}{\partial p} - \frac{Q_2}{L}, \tag{1}$$

where t is time, $\mathbf{V}$ is the horizontal wind vector, ∇ is the horizontal gradient operator, ω is the pressure velocity, p is the pressure, and L is the latent heat of condensation.

To identify the effects of scale interactions, each variable was decomposed into oscillations of the LFBS (>90 days, denoted by an overbar), the ISO [including the 10–30-day (double-prime) and 30–90-day (prime) modes] and the synoptic-scale (<10 days, marked by an asterisk) components through applying the Lanczos bandpass filter[45] to long-term time series of variables at each grid cell. Taking the variables of vertical motion and specific humidity as an example,

$$\omega = \bar{\omega} + \omega' + \omega'' + \omega^*,$$

and

$$q = \bar{q} + q' + q'' + q^*.$$

Then, the vertical moisture advection can be further expressed as follows:

$$\begin{aligned} -\omega\frac{\partial q}{\partial p} = &-\bar{\omega}\frac{\partial \bar{q}}{\partial p} - \omega'\frac{\partial \bar{q}}{\partial p} - \omega''\frac{\partial \bar{q}}{\partial p} - \omega^*\frac{\partial \bar{q}}{\partial p} - \bar{\omega}\frac{\partial q'}{\partial p} \\ &- \omega'\frac{\partial q'}{\partial p} - \omega''\frac{\partial q'}{\partial p} - \omega^*\frac{\partial q'}{\partial p} - \bar{\omega}\frac{\partial q''}{\partial p} - \omega'\frac{\partial q''}{\partial p} - \omega''\frac{\partial q''}{\partial p} \\ &- \omega^*\frac{\partial q''}{\partial p} - \bar{\omega}\frac{\partial q^*}{\partial p} - \omega'\frac{\partial q^*}{\partial p} - \omega''\frac{\partial q^*}{\partial p} - \omega^*\frac{\partial q^*}{\partial p} \end{aligned} \tag{2}$$

The first four terms on the right-hand side of Eq. (2) represent the vertical transport of $\bar{q}$ by various timescale components—namely, the LFBS, the two ISO modes, and the < 10-day disturbances, respectively. The 5th to 8th and 9th to 12th terms describe the vertical moisture transport caused by

Table 1 | Details of the S2S models' real-time forecast and reforecast data

Model	Forecast range (days)	Model resolution	Forecast frequency	Ensemble size for real time	Ensemble size for reforecast	Reforecast period
CMA	0–60	T266, L56	2/week	4	4	2007–2021
ECCC	0–32	0.35° × 0.35°, L45	1/week	21	4	1998–2017
ECMWF	0–46	Tco639/Tco319, L137	2/week	51	11	2002–2021
HMCR	0–61	1.1° × 1.4°, L28	1/week	20	10	1990–2015
IAP-CAS	0–65	C96, L32	Daily	4	4	1999–2018
NCEP	0–44	T126, L64	Daily	16	4	1999–2010

ascending motions with different timescales working on the 30–90-day and 10–30-day moisture fields, respectively. The last four terms indicate the transport of synoptic moisture perturbations by the vertical flows associated with the LFBS, the 30–90-day ISO, the 10–30-day ISO, and the synoptic eddy.

Wave activity flux

The wave activity flux (WAF)[46], formulated as Eq. (3), was used to examine the propagation of the intraseasonal Rossby wave train:

$$\mathrm{W}=\frac{p\cos\phi}{2|\mathbf{U}|}\begin{pmatrix}\frac{U}{a^2\cos\phi}\left[\left(\frac{\partial\psi'}{\partial\lambda}\right)^2-\psi'\frac{\partial^2\psi'}{\partial\lambda^2}\right]+\frac{V}{a^2\cos\phi}\left[\frac{\partial\psi'}{\partial\lambda}\frac{\partial\psi'}{\partial\phi}-\psi'\frac{\partial^2\psi'}{\partial\lambda\partial\phi}\right]\\ \frac{U}{a^2\cos\phi}\left[\frac{\partial\psi'}{\partial\lambda}\frac{\partial\psi'}{\partial\phi}-\psi'\frac{\partial^2\psi'}{\partial\lambda\partial\phi}\right]+\frac{V}{a^2\cos\phi}\left[\left(\frac{\partial\psi'}{\partial\phi}\right)^2-\psi'\frac{\partial^2\psi'}{\partial\phi^2}\right]\end{pmatrix},\tag{3}$$

where **W** is the WAF; ϕ, λ and a represent the latitude, longitude and Earth's radius, respectively; p = (pressure/1000 hPa); $\mathbf{U}=(U,V)$ is the climatological seasonal mean of the basic flow; and ψ denotes the stream function. A prime denotes the 30–90-day component; hence, **W** represents the WAF associated with 30–90-day variability. When the perturbation component is calculated using the 10–30-day filtered data, **W** then measures the WAF for the 10–30-day variability.

Data availability

The CPC precipitation data are available from NOAA's Physical Sciences Laboratory at https://downloads.psl.noaa.gov/Datasets/cpc_global_precip/. The ERA5 data are available from the Copernicus Climate Change Service (C3S) Climate Data Store (CDS) at https://cds.climate.copernicus.eu/#!/search?text=ERA5&type=dataset. The JRA-55 data were obtained from the National Center for Atmospheric Research (NCAR) at http://rda.ucar.edu/datasets/ds628.0/. The S2S database is hosted at ECMWF as an extension of the TIGGE database, at https://apps.ecmwf.int/datasets/data/s2s/. The Niño3.4 SST index and OLR data were obtained from NOAA, at https://psl.noaa.gov/gcos_wgsp/Timeseries/Data/nino34.long.data and https://psl.noaa.gov/data/gridded/data.olrcdr.interp.html, respectively.

Code availability

The data in this study is analyzed with NCAR Command Language (NCL; http://www.ncl.ucar.edu/). The relevant codes in this work are available, upon request, from the corresponding author PC.

Received: 3 June 2024; Accepted: 15 October 2024;
Published online: 23 October 2024

References

1. Hong, C.-C. et al. Causes of 2022 Pakistan flooding and its linkage with China and Europe heatwaves. *npj Clim. Atmos. Sci.* **6**, 163 (2023).
2. Li, B. et al. Middle East warming in spring enhances summer rainfall over Pakistan. *Nat. Commun.* **14**, 7635 (2023).
3. Dunstone, N. et al. Windows of opportunity for predicting seasonal climate extremes highlighted by the Pakistan floods of 2022. *Nat. Commun.* **14**, 6544 (2023).
4. Malik, I., Singh Chuphal, D., Vegad, U. & Mishra, V. Was the extreme rainfall that caused the August 2022 flood in Pakistan predictable? *Environ. Res. Clim.* **2**, 041005 (2023).
5. Doi, T., Behera, S. K. & Yamagata, T. Seasonal predictability of the extreme Pakistani rainfall of 2022 possible contributions from the northern coastal Arabian Sea temperature. *npj Clim. Atmos. Sci.* **7**, 13 (2024).
6. Adnan, S., Ullah, K. & Shouting, G. Investigations into precipitation and drought climatologies in South Central Asia with special focus on Pakistan over the period 1951–2010. *J. Clim.* **29**, 6019–6035 (2016).
7. Wang, Z. et al. Tibetan Plateau heating as a driver of monsoon rainfall variability in Pakistan. *Clim. Dyn.* **52**, 6121–6130 (2019).
8. Ullah, W. et al. Observed linkage between Tibetan Plateau soil moisture and South Asian summer precipitation and the possible mechanism. *J. Clim.* **34**, 361–377 (2021).
9. Hunt, K. M. R., Turner, A. G. & Shaffrey, L. C. Extreme daily rainfall in Pakistan and North India: scale interactions, mechanisms, and precursors. *Mon. Weather Rev.* **146**, 1005–1022 (2018).
10. Hussain, M. S., Kim, S. & Lee, S. On the relationship between Indian Ocean Dipole events and the precipitation of Pakistan. *Theor. Appl. Climatol.* **130**, 673–685 (2017).
11. Iqbal, A. & Hassan, S. A. ENSO and IOD analysis on the occurrence of floods in Pakistan. *Nat. Hazards* **91**, 879–890 (2018).
12. Li, B., Zhou, L., Qin, J. & Murtugudde, R. Increase in intraseasonal rainfall driven by the Arabian Sea warming in recent decades. *Geophys. Res. Lett.* **49**, e2022GL100536 (2022).
13. Roxy, M. K. et al. A threefold rise in widespread extreme rain events over central India. *Nat. Commun.* **8**, 708 (2017).
14. He, C., Zhou, T., Zhang, L., Chen, X. & Zhang, W. Extremely hot East Asia and flooding western South Asia in the summer of 2022 tied to reversed flow over Tibetan Plateau. *Clim. Dyn.* **61**, 2103–2119 (2023).
15. Ma, Y. et al. Different characteristics and drivers of the extraordinary Pakistan rainfall in July and August 2022. *Remote Sens.* **15**, 2311 (2023).
16. Nanditha, J. S. et al. The Pakistan flood of August 2022: causes and implications. *Earth's Future* **11**, e2022EF003230 (2023).
17. Otto, F. E. L. et al. Climate change increased extreme monsoon rainfall, flooding highly vulnerable communities in Pakistan. *Environ. Res. Clim.* **2**, 025001 (2023).
18. Tang, S. et al. Linkages of unprecedented 2022 Yangtze River Valley heatwaves to Pakistan flood and triple-dip La Niña. *npj Clim. Atmos. Sci.* **6**, 44 (2023).
19. Hong, C.-C., Hsu, H.-H., Lin, N.-H. & Chiu, H. Roles of European blocking and tropical-extratropical interaction in the 2010 Pakistan flooding. *Geophys. Res. Lett.* **38**, L13806 (2011).
20. Lau, W. K. M. & Kim, K.-M. The 2010 Pakistan flood and Russian heat wave: teleconnection of hydrometeorological extremes. *J. Hydrometeorol.* **13**, 392–403 (2012).
21. You, Y., Ting, M. & Michela, B. Climate warming contributes to the record-shattering 2022 Pakistan rainfall. *npj Clim. Atmos. Sci*. **7**, 89 (2024).

22. Hunt, K. M. R., Turner, A. G. & Schiemann, R. K. H. How interactions between tropical depressions and western disturbances affect heavy precipitation in South Asia. *Mon. Weather Rev.* **149**, 1801–1825 (2021).
23. Murakami, M. Analysis of the deep convective activity over the Western Pacific and Southeast. *J. Meteor. Soc. Jpn.* **62**, 88–108 (1984).
24. Lau, K.-M. & Chan, P. H. Aspects of the 40–50 day oscillation during the northern summer as inferred from outgoing longwave radiation. *Mon. Weather Rev.* **114**, 1354–1367 (1986).
25. Wang, B., Webster, P. J. & Teng, H. Antecedents and self-induction of active-break South Asian monsoon unraveled by satellites. *Geophys. Res. Lett.* **32**, L04704 (2005).
26. Lee, J.-Y. et al. Real-time multivariate indices for the boreal summer intraseasonal oscillation over the Asian summer monsoon region. *Clim. Dyn.* **40**, 493–509 (2013).
27. Hsu, P.-C., Lee, J.-Y. & Ha, K.-J. Influence of boreal summer intraseasonal oscillation on rainfall extremes in southern China. *Int. J. Climatol.* **36**, 1403–1412 (2016).
28. Hsu, P.-C. et al. Multiscale interactions driving the devastating floods in Henan Province, China during July 2021. *Weather Clim. Extrem.* **39**, 100541 (2023).
29. Chen, G., Ling, J., Lin, Z., Xiao, Z. & Li, C. Role of tropical-extratropical interactions in the unprecedented 2022 extreme rainfall in Pakistan: a historical perspective. *Atmos. Res.* **291**, 106817 (2023).
30. Lu, R.-Y., Oh, J.-H. & Kim, B.-J. A teleconnection pattern in upper-level meridional wind over the North African and Eurasian continent in summer. *Tellus* **54**, 44–55 (2002).
31. Mahendra, N., Chilukoti, N. & Chowdary, J. S. The increased summer monsoon rainfall in Northwest India: Coupling with the Northwestern Arabian Sea warming and modulated by the Silk Road Pattern since 2000. *Atmos. Res.* **297**, 107094 (2024).
32. Kikuchi, K. The boreal summer intraseasonal oscillation (BSISO): a review. *J. Meteor. Soc. Jpn.* **99**, 933–972 (2021).
33. Xu, P., Wang, L. & Ming, J. Central Asian precipitation extremes affected by an intraseasonal planetary wave pattern. *J. Clim.* **35**, 2603–2616 (2022).
34. Yang, J., Zhu, T. & Vitart, F. An extratropical window of opportunity for subseasonal prediction of East Asian summer surface air temperature. *npj Clim. Atmos. Sci.* **6**, 46 (2023).
35. Vitart, F. et al. The subseasonal to seasonal (S2S) prediction project database. *Bull. Am. Meteorol. Soc.* **98**, 163–173 (2017).
36. Singh, B., Ehsan, M. A. & Robertson, A. W. Calibrated probabilistic sub-seasonal forecasting for Pakistan's monsoon rainfall in 2022. *Clim. Dyn*. **62**, 3375–3393 (2024).
37. Mariotti, A. et al. Windows of opportunity for skillful forecasts subseasonal to seasonal and beyond. *Bull. Am. Meteorol. Soc.* **101**, E608–E625 (2020).
38. Xie, J., Hsu, P.-C., Hu, Y., Ye, M. & Yu, J. Skillful extended-range forecast of rainfall and extreme events in East China based on deep learning. *Weather Forecast.* **38**, 467–486 (2023).
39. Chen, M. et al. Assessing objective techniques for gauge-based analyses of global daily precipitation. *J. Geophys. Res.* **113**, D04110 (2008).
40. Hersbach, H. et al. The ERA5 global reanalysis. *Q. J. R. Meteorol. Soc.* **146**, 1999–2049 (2020).
41. Kobayashi, S. et al. The JRA-55 reanalysis: general specifications and basic characteristics. *J. Meteor. Soc. Jpn.* **93**, 5–48 (2015).
42. Liebmann, B. & Smith, C. A. Description of a complete (interpolated) outgoing longwave radiation dataset. *Bull. Am. Meteorol. Soc.* **77**, 1275–1277 (1996).
43. Rayner, N. A. et al. Global analyses of sea surface temperature, sea ice, and night marine air temperature since the late nineteenth century. *J. Geophys. Res*. **108**, 4407 (2003).
44. Yanai, M., Esbensen, S. & Chu, J.-H. Determination of bulk properties of tropical cloud clusters from large-scale heat and moisture budgets. *J. Atmos. Sci.* **30**, 611–627 (1973).
45. Duchon, C. E. Lanczos filtering in one and two dimensions. *J. Appl. Meteorol. Climatol.* **18**, 1016–1022 (1979).
46. Takaya, K. & Nakamura, H. A formulation of a phase-independent wave-activity flux for stationary and migratory quasi-geostrophic eddies on a zonally varying basic flow. *J. Atmos. Sci.* **58**, 608–627 (2001).

Acknowledgements

The valuable feedback from three anonymous reviewers is greatly appreciated for significantly improving the quality of this study. This study was supported by the National Natural Science Foundation of China (42225502). J.-Y.L. was supported by the National Research Foundation of Republic of Korea (NRF-2022M3K3A1097082) and the Institute for Basic Science (IBS), Republic of Korea, under IBS-R028-D1. A.G.T. was supported by the National Centre for Atmospheric Science through the NERC National Capability International Programmes Award (NE/X006263/1). We also acknowledge the High Performance Computing Center of Nanjing University of Information Science and Technology for their support of this work.

Author contributions

P.C.H. and J.X. led this study, with all authors contributing to the research methods and interpretation of the results. J.X. analyzed the results and prepared the figures. J.X. and P.C.H. drafted the manuscript, and other authors contributed to its writing.

Competing interests

The authors declare no competing interests.

Additional information

Supplementary information The online version contains supplementary material available at https://doi.org/10.1038/s41612-024-00809-9.

Correspondence and requests for materials should be addressed to Pang-Chi Hsu.